Segmented up-bending of the Arabian continental plate revealed by Pn attenuation tomography

Geng Yang[1,2], Ling Chen[2,3], Lian-Feng Zhao[1,4], Xiao-Bi Xie[5], and Zhen-Xing Yao[1]

[1] Key Laboratory of Earth and Planetary Physics, Institute of Geology and Geophysics, Chinese Academy of Sciences, Beijing, China.

[2] College of Earth and Planetary Sciences, University of Chinese Academy of Sciences, Beijing, China.

[3] State Key Laboratory of Lithosphere Evolution, Institute of Geology and Geophysics, Chinese Academy of Sciences, Beijing, China.

[4] Heilongjiang Mohe Observatory of Geophysics, Institute of Geology and Geophysics, Chinese Academy of Sciences, Beijing, China.

[5] Institute of Geophysics and Planetary Physics, University of California at Santa Cruz, CA95064, USA.

Corresponding author: Lian-Feng Zhao (zhaolf@mail.iggcas.ac.cn)
Key Laboratory of Earth and Planetary Physics
Institute of Geology and Geophysics, Chinese Academy of Sciences
19 Beituchengxilu, Chaoyang District, Beijing, 100029, China
Tel. 011-86-10-82998658
Fax 011-86-10-62010846

Key Points:

- A high-resolution broadband Pn attenuation model is obtained beneath the Iranian Plateau.
- Weak Pn attenuation delineates the subduction front of the Arabian Plate and reveals its segmented plate up-bending.
- Post-collision magmatism is likely related to the detachment-related mantle upwelling characterized by strong Pn attenuation.

Abstract

The Zagros orogen in the Iranian Plateau is a natural laboratory in which to investigate the tectonic evolution of the transition from oceanic subduction to continental collision. However, where slab detachment occurred and how slab detachment affects shallower continental subduction remain poorly understood. The formation mechanism of the post-collision magmatism is also unclear. Here, we construct a high-resolution Pn-wave attenuation model for the uppermost mantle beneath the Iranian Plateau and surrounding areas using a newly compiled dataset. Weak Pn attenuation delineates the Arabian Plate front near the Moho discontinuity, extending further toward the subduction direction in the northwestern and southeastern parts, possibly due to the up-bending and underplating of the Arabian lithosphere after the loss of slab pull. The correlations among the surface Miocene-Quaternary volcanism and strong Pn attenuation in the uppermost mantle suggest that asthenospheric materials escaped from slab windows and further feed the post-collision volcanoes.

Keywords: Pn-wave attenuation, Iranian Plateau, Slab detachment, Plate up-bending, Post-collision magmatism, Mantle upwelling

Plain Language Summary

Various geological and geophysical observations show that deep oceanic slabs may have detached one after another from the Arabian continental plate, forming complex plate front beneath the Iranian Plateau. However, the processes of continental subduction and collision remain poorly understood. The formation mechanism of the complex magmatism in the Iranian Plateau is also unclear. The uppermost mantle generally represents the core position of the mantle lid where the rheological variations can characterize the thermal structure. In this study, we conducted high-resolution Pn-wave attenuation tomography for the uppermost mantle beneath the Iranian Plateau, using 23,251 vertical-component waveforms recorded at 291 previous stations and 197 new temporary stations. The resulting images show that the cold Arabian plate is characterized by weak Pn attenuation beneath the Zagros orogen and the strong attenuation anomalies are related to younger magmatism. Combined with previous geological and geochemical observations, our results suggest a successive evolution process under the Iranian Plateau. The ancient Neotethys oceanic plate partially detached from the Arabian continental margin. After the slab break-off at depth, subducted Arabian continental slab rose back and flatten below the overriding plate. Meanwhile, the detachment-related asthenosphere upwelling fed the younger volcanism at the surface.

1 Introduction

Plate convergence processes determine the formation and evolution of plateaus, such as the Iranian, Anatolian, and Tibetan plateaus. When transitioning from oceanic subduction to continental collision, a down-going slab will likely break off and be accompanied by an increase in tensile stress between the deep and shallow parts of the slab, where continental crust subduction produces strong buoyancy at relatively shallow depths (Davies and Blanckenburg, 1995; Kufner et al., 2021). After slab detachment, the subducted continental lithosphere loses the drag force of the deep slab and hence possibly up-bends toward the overriding plate (Li et al., 2013; van Hunen and Allen, 2011). In this situation, asthenospheric flow is likely triggered around the broken edges of the plate (e.g., Guivel et al., 2006; Kundu and Gahalaut, 2011). Although numerical modeling can simulate the processes of continental subduction and collision (Gao et al., 2023; Li et al., 2013; Magni et al., 2017; van Hunen and Allen, 2011), understanding its geodynamic complexity requires further information gathered from geological and geophysical observations, such as seismic velocity and attenuation tomography (Stern et al., 2021).

The Zagros orogen, a fold-thrust belt in the Iranian Plateau, is in the middle part of the famous Alpine-Zagros-Himalayan convergent zones after the Neotethys Ocean closure and the Arabia-Eurasia collision (Figure 1) (e.g., Chemenda et al., 2000; Li et al., 2013; Stern et al., 2021). Seismic tomography revealed that the Neotethyan plate subducted northward and that the deep oceanic slab partially detached from the Arabian continental margin (e.g., Alinaghi et al., 2007; Hafkenscheid et al., 2006; Mahmoodabadi et al., 2019; Manaman and Shomali, 2010; Rahmani et al., 2019; Shomali et al., 2011). However, the inconsistent imaging results lead to controversy over the detachment locations. The deep oceanic slab may have detached under the northwestern and southeastern Zagros orogen, avoiding the central Zagros (e.g., Agard et al., 2011; Alinaghi et al., 2007; Hafkenscheid et al., 2006). Otherwise, an updated velocity model for the Iranian Plateau observed similar discontinuous

high-velocity anomalies under the central Zagros (Mahmoodabadi et al., 2019). Although the surface topographic relief is not sensitive to deep plate kinematic processes, shallow Arabian lithosphere tectonics strongly react to slab detachment at depth, such as plate up-bending and underplating (Li et al., 2013; van Hunen and Allen, 2011). Therefore, investigating the detailed structure of the upper mantle is an effective way to understand the entire subduction and collision processes.

Both plate subduction and collision led to active magmatism and formed the Urumieh-Dokhtar magmatic arc (UDMA) along the subduction front of the Arabian Plate (Verdel et al., 2011). The UDMA extends from the Talesh Caucasus and Alborz Mountains in the northwest to the Makran subduction region in the southeast. Zircon U–Pb age measurements show that the Urumieh-Dokhtar magmatism was most active during the Eocene and Oligocene (55-25 Ma) (Chiu et al., 2013 and references therein) and was controlled by Neotethyan oceanic subduction (e.g., Asadi et al., 2014; Babazadeh et al., 2017). Oceanic subduction was terminated by a continental collision between the Arabian and Iranian plates, but volcanism in the northwestern and southeastern parts of the UDMA continued to the Miocene-Quaternary (Chiu et al., 2013). To understand the post-collisional magmatism in the UDMA, several models have been proposed but are controversial, including slab rollback (e.g., Babazadeh et al., 2017), slab break-off (e.g., Ghalamghash et al., 2016; Jahangiri, 2007; Omrani et al., 2008), changes in subduction angle (Shahabpour, 2007), and crustal thickening caused by oblique and diachronous collision (Chiu et al., 2013). Exploring the detailed lithospheric thermal structure and linking the deep dynamic processes with surface volcanism is key to recognizing the magmatic evolution.

Compared with seismic velocity, seismic attenuation is more sensitive to temperature, partial melting and fluid (e.g., Artemieva et al., 2004; Boyd et al., 2004; He et al., 2021; Zhu et al., 2013). In this study, we construct a Pn-wave attenuation model in and around the Iranian Plateau to detect the boundary of the Arabian subduction front and the potential magma sources in the uppermost mantle.

The layered results, including the subcrustal lithospheric thermal structure obtained in this study, crustal thermal anomalies from strong Lg attenuation (Yang et al., 2023) and surface volcanic rocks, suggest a successive process from deep geodynamics, including slab break-off, plate up-bending and mantle upwelling, to crustal heat storage and transmission as well as volcanic eruption near the Arabian subduction front.

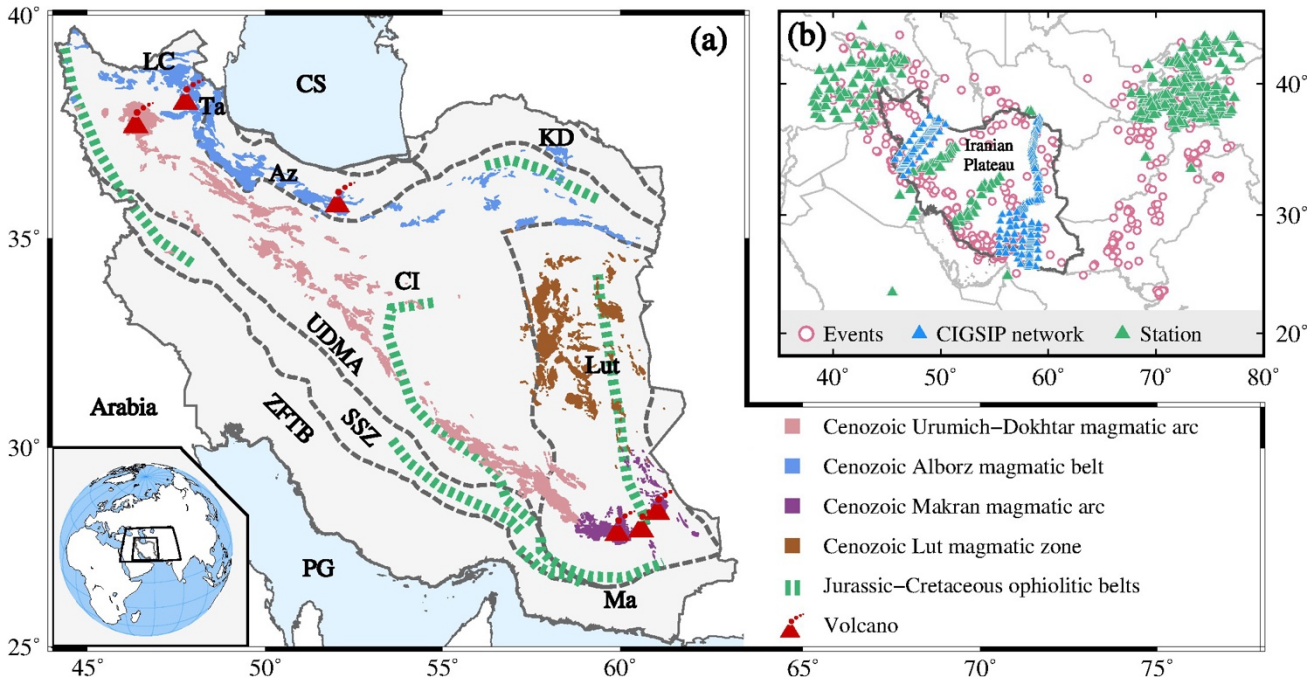

Figure 1. Maps showing the major geological blocks and magmatic belts in the Iranian Plateau (a) and the locations of stations and earthquakes (b). CS: Caspian Sea; PG: Persian Gulf; OS: Oman Sea; LC: Lesser Caucasus Mountains; Ta=Talesh Mountains; Az: Alborz Mountains; KD: Kopet-Dogh Mountains; CI: Central Iranian Basins; Lut: Lut Blocks; UDMA: Urumieh-Dokhtar magmatic arc; ZFTB: Zagros Fold-Thrust Belt; Ma: Makran region; SSZ: Sanandaj-Sirjan Zone; CIGSIP: The China-Iran Geological and Geophysical Survey in the Iranian Plateau during 2013-2018.

2 Data and methods

A total of 23,251 vertical-component waveforms were collected from 594 crustal earthquakes recorded at 488 broadband stations in and around the Iranian Plateau, where 291 stations belong to regional networks (see Data Availability Statement), and 197 new stations that belong to three temporary seismic networks in western and eastern Iran established by the "China-Iran Geological and Geophysical Survey in the Iranian Plateau (CIGSIP)" project during 2013-2018 (Gao et al., 2022; Sadeghi-Bagherabadi et al., 2018; Wang et al., 2022; Wu et al., 2021). Earthquakes that occurred above the Moho (Laske et al., 2013) with known focal mechanisms were selected from the Harvard Centroid Moment Tensor (CMT) catalog (Ekstrom et al., 2012) to calculate the radiation patterns of Pn-waves. The earthquake sizes were confined within a magnitude range of $4.3 \leq m_b \leq 6.5$. Figure S1 illustrates 72 waveforms from the three temporary CIGSIP networks, bandpass filtered between 0.5 and 8.0 Hz. The Pn signals with different propagation paths were clearly recorded. Detailed station and earthquake information is listed in Tables S1 and S2. We extracted Pn-wave spectral amplitude from these vertical component waveforms and conducted Pn-wave attenuation tomography following Zhao et al. (2015) and Yang et al. (2022). For detailed methodology, please refer to Text S1 in Supporting Information.

3 Results

A high-resolution Pn-wave attenuation model was constructed for the Iranian Plateau at 42 individual frequencies between 0.5 and 20.0 Hz. Lateral variations in the Pn attenuation are remarkable, as shown in the selected Q_{Pn} images at 1.0, 2.0, 3.0 and 5.0 Hz (Figure S7). The large-scale attenuation structures are generally stable at individual frequencies, and the Q_{Pn} value increases with frequency. Based on the Pn attenuation model, the Q_{Pn} value versus frequency is statistically obtained in six major geological units, including the Eurasian and Arabian Plates, the Afghan block, and the Iranian,

Pamir and Anatolian Plateaus (Figure S8). The Q_{Pn}-frequency curves seem to be parabolas between 0.5 and 20.0 Hz, where the Anatolian and Iranian Plateaus exhibit relatively lower Q_{Pn} values. Comparing the frequency dependencies of different units, the portion between 0.5 and 5.0 Hz can clearly distinguish different units (Figure 2a). However, outside of the dominating band, the Q_{Pn} curves are mixed closer and strongly dependent on frequency rather than tectonic features. Therefore, the frequency range from 0.5-5.0 Hz was selected as the dominant band for the Pn attenuation model.

The broadband attenuation model was calculated by the logarithmic average of Q_{Pn} values between 0.5 and 5.0 Hz (Figure 2b). The lateral variation in the broadband Pn attenuation is almost consistent with those at the individual frequencies (Figure S7), and also exhibits high consistency with previous attenuation and velocity imaging results for the uppermost mantle (see the Text S2 in Supporting Information). The broadband Q_{Pn} value extends from 10 to 700, where the Arabian Plate, the Eurasia Plate and the Makran subduction region are characterized by weak attenuation in the uppermost mantle (Q_{Pn}>500) and high velocities from previous tomographic results (e.g., Al-Lazki et al., 2014; Amini et al., 2012; Lü et al., 2012; Lü et al., 2017; Pei et al., 2011). From west to east, the Anatolian Plateau, the Iranian Plateau, the Afghan Block and the Pamir Plateau exhibit overall lower Q_{Pn} (Q_{Pn}<250), which is aligned with the Pn low-velocity anomalies (e.g., Al-Lazki et al., 2014; Amini et al., 2012; Lü et al., 2017; Pei et al., 2011). With contribution from the new CIGSIP stations, dense ray-path coverage, and accurate measurement of Pn amplitude, more details were discovered in our high-resolution Pn attenuation model. Inside the Iranian Plateau (Figure 2c), the high-Q_{Pn} value in the uppermost mantle beneath the Zagros orogen indicates the cold Arabian continental lithosphere, where the northwestern and southeastern parts are characterized by higher Q_{Pn} values than the middle part and extend farther to the northeast (H1 and H2). Along the UDMA, two low-Q_{Pn} anomalies are revealed beneath the northwestern end near the Alborz Mountains and the southeastern UDMA near the Makran region (L1 and L2). The Alborz and Kopet-Dogh Mountains show low-Q_{Pn} features and

crop out in the Alborz volcanic rocks. Similarly, strong Pn attenuation was observed beneath the Lut magmatic zone in the eastern Iranian Plateau.

The uncertainty of our tomographic inversion is small based on the bootstrapping technique (Efron, 1983). The synthetic test results also confirm the main structural features are robust, and both the shapes and magnitudes of the given anomalies can be well retrieved (see the Text S3 in Supporting Information).

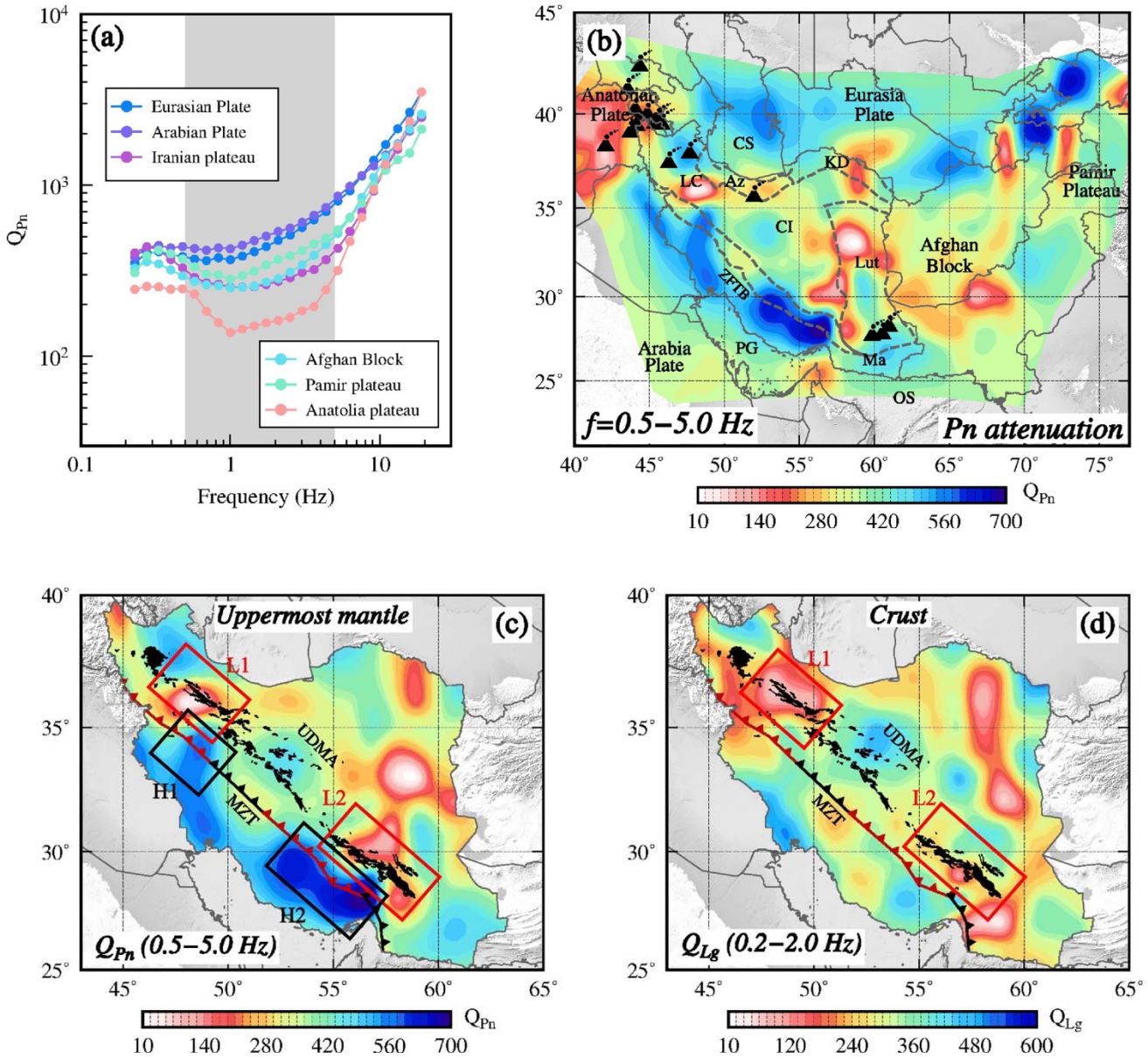

Figure 2. Maps showing broadband Pn-wave attenuation tomographic results. (a) Comparison of the frequency-dependent Q_{Pn} of selected blocks. The shaded areas highlight the dominating frequency band of 0.5-5.0 Hz. (b) Broadband Q_{Pn} map from 0.5-5.0 Hz. The volcanoes are marked as black triangles. (c) Uppermost mantle Q_{pn} image inside the Iranian Plateau. (d) Crustal Q_{Lg} images inside the Iranian Plateau (Yang et al., 2023). The black areas represent the locations of Cenozoic Urumieh-Dokhtar volcanic rock outcrops. The Main Zagros Thrust (MZT) represents the suture of two continental plates, along which the Neotethys subducted beneath central Iran. The possible slab break-off regions (red segments) were suggested by results from seismic tomography and geochemical observations (Agard et al., 2011; Hafkenscheid et al., 2006; Omrani et al., 2008). The low-Q_{pn} and low-Q_{Lg} zones L1 and L2 and the high-Q_{pn} zones H1 and H2 are revealed beneath the UDMA and Zagros orogen, respectively.

4 Discussion

4.1 Comparison with crustal attenuation model

The crustal Lg-wave attenuation was investigated in and around the Iranian Plateau using the same dataset (Figure 2d) (Yang et al., 2023). A two-layer attenuation model can be obtained for both the crust and uppermost mantle in this region. Low crustal Q_{Lg} and high uppermost mantle Q_{Pn} values are observed beneath the Zagros orogen and are related to the active crustal extrusion deformation during the Arabia-Iran collision and cold plate subduction, respectively. Some strong attenuation anomalies can be simultaneously observed in both the uppermost mantle and crust. For example, two anomalies with crustal low-Q_{Lg} and uppermost mantle low-Q_{Pn} values are revealed beneath the northwestern and southeastern UDMA (L1 and L2 in Figures 2c and 2d), suggesting upwellings from the uppermost mantle to the crust, which is consistent with previous velocity and attenuation

tomographic images (e.g., Amini et al., 2012; Hearn, 2022; Kaviani et al., 2022; Pei et al., 2011). Additionally, the Lut magmatic belt with low-Q_{Lg} and low-Q_{Pn} values suggests magmatic accumulations in the crust and uppermost mantle (see Text S4 in Supporting Information for detailed discussion).

4.2 Segmented up-bending/underplating of the Arabian continental plate

The Arabian continental subduction followed the subduction of the Neotethyan oceanic lithosphere into the trench. Upper mantle P- and S-wave velocity tomography revealed high-velocity anomalies down to a 600 km depth beneath Iran (e.g., Alinaghi et al., 2007; Hafkenscheid et al., 2006; Mahmoodabadi et al., 2019), where the shallower high-velocity anomaly (< 200 km) was interpreted as the Arabian mantle lithosphere and the high-velocity anomaly below ~200 km was interpreted as the remaining Neotethyan oceanic slab. The detached slabs below ~300 km was revealed under the northwestern and southeastern Zagros orogen, but beneath the central Zagros, the high-velocity anomalies at depths of 200-500 km were still connected to the shallower Arabian Plate (Agard et al., 2011; Hafkenscheid et al., 2006). Therefore, the subducted deep slab can be partially detached under the Iranian Plateau (red dashed lines in Figure 3). According to the ages of the adakitic rocks, the slab break-off occurred during ~40-30 Ma under northwestern Iran, skipped central Iran, and propagated southeast to Makran from 10-5 Ma to the present (Agard et al., 2011; Hafkenscheid et al., 2006; Omrani et al., 2008). However, the detachment locations from different velocity tomographic images were not uniform (e.g., Mahmoodabadi et al., 2019). These disputes may be resolved by the characteristics of the shallower continental lithosphere.

The breaking of a subducted slab has profound impacts on the thermal structure of the mantle wedge. The possible slab break-off regions are highlighted using the red dashed lines in Figure 3 (Agard et al., 2011; Alinaghi et al., 2007; Omrani et al., 2008). The slab detachment zones beneath the

northwestern and southeastern Zagros are consistent with convex high-Q_{Pn} anomalies in the uppermost mantle. Numerical simulations indicate that after slab break-off at depth, the subducted continental plate will rise back or up-bend toward the surface under the action of buoyancy at shallower depths and further flatten below the overriding plate (e.g., Li et al., 2013; Magni et al., 2017; van Hunen and Allen, 2011). Compared with the central Zagros, the northwestern and southeastern Arabian lithosphere with stronger high-Q_{Pn} anomalies extends farther in the direction of subduction, which corresponds well with the plate up-bending process and indicates the Arabian Plate may have bent upward above the positions of the slab detachment, making the high-Q_{Pn} anomalies extend forward near the Moho (Figure 3). The rising of the subducted continental crust forces the mantle wedge to progressively migrate away from the trench (Magni et al., 2017). Beneath the Zagros orogen, the northwestern and southeastern Arabian Plates with high-Q_{Pn} migrate as far as ~150 and ~70 km north of the main suture during approximately 30 and 10 Myr (Omrani et al., 2008), respectively, which aligns with the migration velocity of ~200 km/35 Myr suggested by numerical simulation (Magni et al., 2017).

The Moho depth map obtained from the receiver function showed thicker crusts (>50 km) beneath northwestern and southeastern Zagros (Mooney, 2015; Taghizadeh-Farahmand et al., 2015), which corresponded to the stronger high-Q_{Pn} anomalies and the possible plate up-bending zones of the Arabian lithosphere (Figure S13). Furthermore, the thicker crustal structures in northwestern and southeastern Zagros were also supported by other Moho models based on surface wave tomography (Kaviani et al., 2020; Manaman et al., 2011), despite some differences. This indicated the overlying crusts in northwestern and southeastern Zagros are likely to thicken under the compressive force from plate underplating. Various studies have demonstrated slab detachment and plate underplating occurred beneath the northwestern and southeastern Zagros orogen (Agard et al., 2011; Alinaghi et al., 2007; Hafkenscheid et al., 2006).

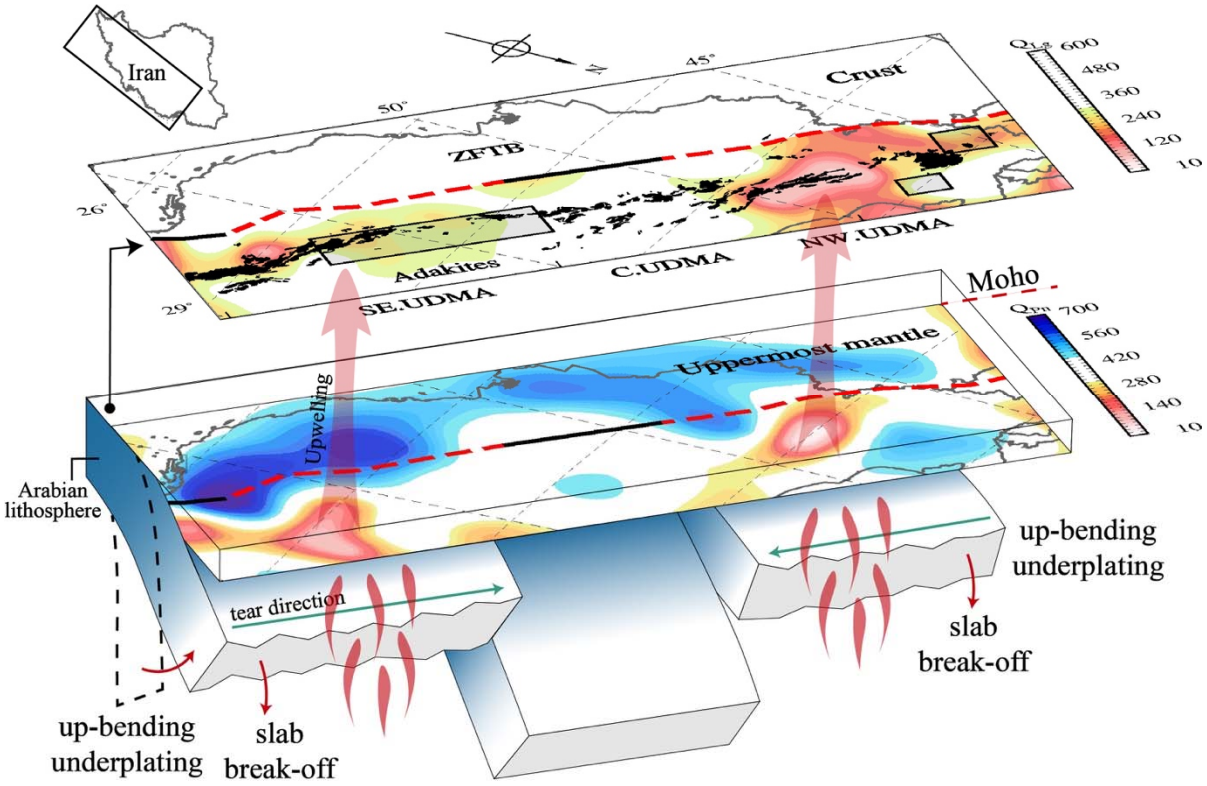

Figure 3. Schematic diagram showing the dynamics of slab break-offs, plate up-bending and magmatic upwellings beneath the UDMA. Broadband Q_{Lg} and Q_{Pn} maps are shown above and below, respectively. In the crustal attenuation map, the Cenozoic volcanic rock outcrops in the UDMA are filled as black areas. Adakitic rocks were observed in the northwestern and southeastern UDMA and marked as shaded areas (Ghalamghash et al., 2016; Jahangiri, 2007; Omrani et al., 2008). The MZT (black lines and red dashed lines) represents the suture of two continental plates, along which the Neotethys subducted beneath central Iran. The red dashed segments represent the possible slab break-off regions (Agard et al., 2011; Alinaghi et al., 2007; Omrani et al., 2008). The red arrows indicate that two mantle upwellings escaped upward from slab tears and intruded into the upper mantle and crust to feed the younger volcanism at the surface.

4.3 Detachment-controlled mantle upwelling

The linear UDMA represents a subduction-related magmatic belt and extends approximately 1500 km along the continental subduction front. From the Late Cretaceous to Paleogene, the UDMA records abundant eruptions of low-K tholeiitic and calc-alkaline magmas, retaining voluminous volcanic successions with minor intrusive rocks (Chiu et al., 2017). The Eocene–Oligocene volcanoes in the UDMA were fed by the mantle wedge melting induced by the Neotethys subduction (e.g., Asadi et al., 2014), but the formation mechanism of late Cenozoic magmatism is controversial. Several interpretation models have been proposed, including slab rollback (e.g., Babazadeh et al., 2017), slab break-off (e.g., Ghalamghash et al., 2016; Jahangiri, 2007; Omrani et al., 2008), changes in subduction angle (Shahabpour, 2007), and crustal thickening (Chiu et al., 2013).

Figure 4a illustrates the age distribution of igneous rocks along the UDMA (Chiu et al., 2013 and references herein). The magmatism in the central UDMA ceased after ~15 Ma, while the volcanism in the northwestern and southeastern UDMA continued to the Quaternary. In the crust, two low-Q_{Lg} zones are revealed beneath the northwestern and southeastern UDMA, and a high-Q_{Lg} zone appears around the central UDMA (Figure 2d). Similarly, two low-Q_{Pn} characteristics are shown in the uppermost mantle but have a certain shrinkage compared to the crustal strong attenuation anomalies (Figure 2c). As illustrated in Figures 4b and 4c, both the Q_{Lg} and Q_{Pn} curves along the UDMA exhibit two remarkably strong attenuation zones, indicating potential magmatic accumulations. The lower velocity zones near the northwestern and southeastern UDMA were also revealed in previous Pn and Sn velocity tomography (e.g., Al-Lazki et al., 2004; Pei et al., 2011). The lateral variations in the thermal structure beneath the UDMA indicate complex origins of younger magmatism. From northwest to southeast, the young-old-young age variation of the igneous rocks corresponds well to the strong-weak-strong attenuation feature, the continental plate up-bending zones and the slab break-off regions. Therefore, the Miocene-Quaternary volcanism in the northwestern and southeastern UDMA

may have been triggered by slab detachment at depth (Ghalamghash et al., 2016; Jahangiri, 2007; Omrani et al., 2008). The low-Q_{Lg} and low-Q_{Pn} anomalies imply two possible magma channels under the northwestern and southeastern UDMA (Figures 4b and 4c). The two asthenospheric upwellings escaped upward from the slab tears, intruded into the upper mantle and crust, and further fed the younger volcanism at the surface. However, the magmatism in the central UDMA has not been reactivated by a detachment-related magmatic source since ~15 Ma. Geochemical surveys also found adakitic magmas in the northwestern and southeastern UDMA in response to the melting of mafic material at depth under high-temperature conditions and possible slab break-off (Ghalamghash et al., 2016; Jahangiri, 2007; Omrani et al., 2008). Crustal thickening may also lead to magma compositional changes from calc-alkaline to adakitic (e.g., Chiu et al., 2013). However, the two magmatic sources in the uppermost mantle are distributed in clusters rather than along the collision strike, suggesting the younger magmatism was likely fed by mantle upwelling (Figure 3).

The migrations of Miocene-Quaternary volcanism are clearly identifiable in the UDMA. The volcanic rocks in the northwestern and southeastern UDMA become younger toward the central UDMA (green arrows in Figures 3 and 4a). Volcanism migrations with different directions are difficult to explain in a steady-state subduction scenario or a simple oblique continental collision (e.g., Ferrari, 2004; Wortel and Spakman, 2000). If slab break-off is used to interpret the formation of the post-collision volcanism, the along-arc migration of magmatism may support the southeastward and northwestward propagations of the slab tears beneath the northwestern and southeastern Zagros orogen (Li et al., 2013; van Hunen and Allen, 2011). Similar migration phenomena of break-off and volcanism have also been observed in multiple places, such as the northeastern Tibetan Plateau and central Mexico (Ferrari, 2004; Yang et al., 2021).

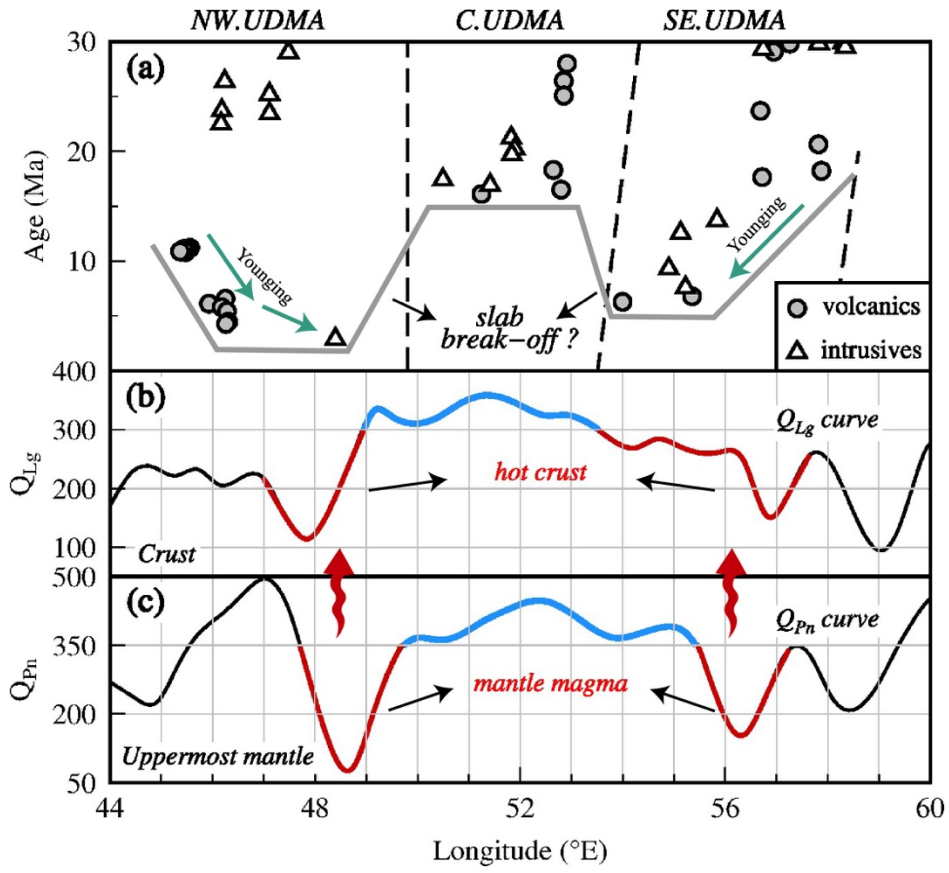

Figure 4. Distributions of magmatic rock ages and attenuation Q along the UDMA. (a) Age versus space plot of dated samples from the UDMA, modified from Chiu et al. (2013). The solid line outlines the age variation in young volcanism. The green arrows indicate the younging directions of magmatism. (b-c) Q_{Lg} and Q_{Pn} curves along the UDMA. The weak and strong attenuation zones are shown in blue and red, respectively. The red arrows suggest potential mantle upwelling related to slab break-off.

5 Conclusions

Combining high-resolution Pn and Lg attenuation models and other observations, we proposed a model for the dynamic processes of slab break-off, plate up-bending/underplating and associated magmatism beneath the transition zone from the Neotethyan subduction to the Arabian collision

(Figure 3). Beneath the Zagros orogen, the high-Q_{Pn} anomalies described the boundary of the Arabian subduction front near the Moho discontinuity, where the northwestern and southeastern parts extended farther toward the subduction direction, which corresponded to slab detachment zones suggested by results from seismic tomography and adakitic rocks (Agard et al., 2011; Hafkenscheid et al., 2006; Omrani et al., 2008). This indicated that after the potential slab break-offs, the northwestern and southeastern Arabian Plates rose back toward the surface under the action of buoyancy at shallower depths. The Arabian Plate further flattens below the overriding plate and forms thick crust structures (>50 km) beneath the northwestern and southeastern Zagros orogen (e.g., Taghizadeh-Farahmand et al., 2015). Affected by continental plate up-bending, the mantle wedge progressively migrated away from the suture of the Arabian and Eurasian Plates. Beneath the northwestern and southeastern Urumieh-Dokhtar magmatic arc, two mantle upwellings with strong attenuation features likely escaped upward from the slab tears, intruded into the upper mantle and crust and further fed the younger Miocene-Quaternary volcanism at the surface. The along-arc migration of Urumieh-Dokhtar volcanism suggests that the deep slab was likely to start breaking near the oceanic subduction zone in Makran and the eastern Mediterranean Sea and further propagated inward.

Data Availability Statement

The waveforms used in this study were collected from the Incorporated Research Institutions for Seismology Data Management Center, the German Research Centre for Geoscience, the International Seismological Centre, the International Federation of Digital Seismograph Networks, and the CIGSIP project (Gao et al., 2022; Sadeghi-Bagherabadi et al., 2018; Wu et al., 2021). The Pn waveforms from the CIGSIP were uploaded to the World Data Centre for Geophysics, Beijing (WDCGB) at http://www.geophys.ac.cn/ArticleDataInfo.asp?MetaId=503. The single- and two-station Pn

amplitude data used in this study and the resulting Pn attenuation model in the Iranian Plateau can be accessed on the WDCGB at http://www.geophys.ac.cn/ArticleDataInfo.asp?MetaId=504 (last accessed April 2023). Certain figures were generated using Generic Mapping Tools (GMT; https://www.generic-mapping-tools.org/).

Acknowledgments

This research was supported by the National Natural Science Foundation of China (91855207, 41630210, U2139206, 41974054, and 41974061). We thank M.Y. Feng for his help in preparing the waveforms from the CIGSIP stations. The CIGSIP project was implemented following the memorandum of understanding (MOU) between IGGCAS and GSI.

References

Agard, P., Omrani, J., Jolivet, L., Whitechurch, H., Vrielynck, B., Spakman, W., MoniÉ, P., Meyer, B., Wortel, R., 2011. Zagros orogeny: a subduction-dominated process. Geological Magazine. 148, 692-725. https://doi.org/10.1017/s001675681100046x

Al-Lazki, A.I., Al-Damegh, K.S., El-Hadidy, S.Y., Ghods, A., Tatar, M., 2014. Pn-velocity structure beneath Arabia–Eurasia Zagros collision and Makran subduction zones. Geological Society, London, Special Publications. 392, 45-60. https://doi.org/10.1144/sp392.3

Al-Lazki, A.I., Sandvol, E., Seber, D., Barazangi, M., Turkelli, N., Mohamad, R., 2004. Pn tomographic imaging of mantle lid velocity and anisotropy at the junction of the Arabian, Eurasian and African plates. Geophysical Journal International. 158, 1024-1040. https://doi.org/10.1111/j.1365-246X.2004.02355.x

Alinaghi, A., Koulakov, I., Thybo, H., 2007. Seismic tomographic imaging of P- and S-waves velocity perturbations in the upper mantle beneath Iran. Geophysical Journal International. 169, 1089-1102. https://doi.org/10.1111/j.1365-246X.2007.03317.x

Amini, S., Shomali, Z.H., Koyi, H., Roberts, R.G., 2012. Tomographic upper-mantle velocity structure beneath the Iranian Plateau. Tectonophysics. 554-557, 42-49. https://doi.org/10.1016/j.tecto.2012.06.009

Artemieva, I.M., Billien, M., Lévêque, J.-J., Mooney, W.D., 2004. Shear wave velocity, seismic attenuation, and thermal structure of the continental upper mantle. Geophysical Journal International. 157, 607-628. https://doi.org/10.1111/j.1365-246X.2004.02195.x

Asadi, S., Moore, F., Zarasvandi, A., 2014. Discriminating productive and barren porphyry copper deposits in the southeastern part of the central Iranian volcano-plutonic belt, Kerman region, Iran: A review. Earth-Science Reviews. 138, 25-46. https://doi.org/10.1016/j.earscirev.2014.08.001

Babazadeh, S., Ghorbani, M.R., Bröcker, M., D'Antonio, M., Cottle, J., Gebbing, T., Carmine Mazzeo, F., Ahmadi, P., 2017. Late Oligocene–Miocene mantle upwelling and interaction inferred from mantle signatures in gabbroic to granitic rocks from the Urumieh–Dokhtar arc, south Ardestan, Iran. International Geology Review. 59, 1590-1608. https://doi.org/10.1080/00206814.2017.1286613

Boyd, O.S., Jones, C.H., Sheehan, A.F., 2004. Foundering lithosphere imaged beneath the Southern Sierra Nevada, California, USA. Science. 305, 660-662. https://doi.org/10.1126/science.1099181

Chemenda, A.I., Burg, J.P., Mattauer, M., 2000. Evolutionary model of the Himalaya-Tibet system: geopoem based on new modelling, geological and geophysical data. Earth and Planetary Science Letters. 174, 397-409. https://doi.org/10.1016/s0012-821x(99)00277-0

Chiu, H.-Y., Chung, S.-L., Zarrinkoub, M.H., Melkonyan, R., Pang, K.-N., Lee, H.-Y., Wang, K.-L., Mohammadi, S.S., Khatib, M.M., 2017. Zircon Hf isotopic constraints on magmatic and tectonic evolution in Iran: Implications for crustal growth in the Tethyan orogenic belt. Journal of Asian Earth Sciences. 145, 652-669. https://doi.org/10.1016/j.jseaes.2017.06.011

Chiu, H.-Y., Chung, S.-L., Zarrinkoub, M.H., Mohammadi, S.S., Khatib, M.M., Iizuka, Y., 2013. Zircon U–Pb age constraints from Iran on the magmatic evolution related to Neotethyan subduction and Zagros orogeny. Lithos. 162-163, 70-87. https://doi.org/10.1016/j.lithos.2013.01.006

Davies, J.H., Blanckenburg, F.v., 1995. Slab breakoff: A model of lithosphere detachment and its test in the magmatism and deformation of collisional orogens. Earth and Planetary Science Letters. 129, 85-102. https://doi.org/10.1016/0012-821X(94)00237-S

Efron, B., 1983. Estimating the error rate of a prediction rule: Improvement on cross-validation. Journal of the American Statistical Association. 78, 316-331. https://doi.org/10.1080/01621459.1983.10477973

Ekstrom, G., Nettles, M., Dziewonski, A.M., 2012. The global CMT project 2004-2010: Centroid-moment tensors for 13,017 earthquakes. Physics of the Earth and Planetary Interiors. 200, 1-9. https://doi.org/10.1016/j.pepi.2012.04.002

Ferrari, L., 2004. Slab detachment control on mafic volcanic pulse and mantle heterogeneity in central Mexico. Geology. 32. https://doi.org/10.1130/g19887.1

Gao, Y., Chen, L., Talebian, M., Wu, Z., Wang, X., Lan, H., Ai, Y., Jiang, M., Hou, G., Khatib, M.M., Xiao, W., Zhu, R., 2022. Nature and structural heterogeneities of the lithosphere control the continental deformation in the northeastern and eastern Iranian plateau as revealed by shear-wave splitting observations. Earth and Planetary Science Letters. 578. https://doi.org/10.1016/j.epsl.2021.117284

Gao, Y., Chen, L., Yang, J., Wang, K., 2023. Rheological Heterogeneities Control the Non-Progressive Uplift of the Young Iranian Plateau. Geophysical Research Letters. 50. https://doi.org/10.1029/2022gl101829

Ghalamghash, J., Mousavi, S.Z., Hassanzadeh, J., Schmitt, A.K., 2016. Geology, zircon geochronology, and petrogenesis of Sabalan volcano (northwestern Iran). Journal of Volcanology and Geothermal Research. 327, 192-207. https://doi.org/10.1016/j.jvolgeores.2016.05.001

Guivel, C., Morata, D., Pelleter, E., Espinoza, F., Maury, R.C., Lagabrielle, Y., Polvé, M., Bellon, H., Cotten, J., Benoit, M., Suárez, M., de la Cruz, R., 2006. Miocene to Late Quaternary Patagonian basalts (46–47°S): Geochronometric and geochemical evidence for slab tearing due to active spreading ridge subduction. Journal of Volcanology and Geothermal Research. 149, 346-370. https://doi.org/10.1016/j.jvolgeores.2005.09.002

Hafkenscheid, E., Wortel, M.J.R., Spakman, W., 2006. Subduction history of the Tethyan region derived from seismic tomography and tectonic reconstructions. Journal of Geophysical Research. 111. https://doi.org/10.1029/2005jb003791

He, X., Zhao, L.F., Xie, X.B., Tian, X., Yao, Z.X., 2021. Weak crust in Southeast Tibetan Plateau revealed by Lg-Wave attenuation tomography: Implications for crustal material escape. Journal of Geophysical Research: Solid Earth. 126. https://doi.org/10.1029/2020jb020748

Hearn, T.M., 2022. Two-dimensional attenuation and velocity tomography of Iran. Geosciences. 12. https://doi.org/10.3390/geosciences12110397

Jahangiri, A., 2007. Post-collisional Miocene adakitic volcanism in NW Iran: Geochemical and geodynamic implications. Journal of Asian Earth Sciences. 30, 433-447. https://doi.org/10.1016/j.jseaes.2006.11.008

Kaviani, A., Paul, A., Moradi, A., Mai, P.M., Pilia, S., Boschi, L., Rümpker, G., Lu, Y., Tang, Z., Sandvol, E., 2020. Crustal and uppermost mantle shear wave velocity structure beneath the Middle East from surface wave tomography. Geophysical Journal International. 221, 1349-1365. https://doi.org/10.1093/gji/ggaa075

Kaviani, A., Sandvol, E., Ku, W., Beck, S.L., Türkelli, N., Özacar, A.A., Delph, J.R., 2022. Seismic attenuation tomography of the Sn phase beneath the Turkish-Iranian Plateau and the Zagros mountain belt. Geosphere. 18, 1377-1393. https://doi.org/10.1130/ges02503.1

Kufner, S.K., Kakar, N., Bezada, M., Bloch, W., Metzger, S., Yuan, X., Mechie, J., Ratschbacher, L., Murodkulov, S., Deng, Z., Schurr, B., 2021. The Hindu Kush slab break-off as revealed by deep structure and crustal deformation. Nat Commun. 12, 1685. https://doi.org/10.1038/s41467-021-21760-w

Kundu, B., Gahalaut, V.K., 2011. Slab detachment of subducted Indo-Australian plate beneath Sunda arc, Indonesia. Journal of Earth System Science. 120, 193-204. https://doi.org/10.1007/s12040-011-0056-7

Laske, G., Masters, G., Ma, Z., Pasyanos, M., 2013. Update on CRUST1.0 – A 1-degree Global Model of Earth's Crust, EGU General Assembly 2013, Vienna, Austria.

Li, Z.-H., Xu, Z., Gerya, T., Burg, J.-P., 2013. Collision of continental corner from 3-D numerical modeling. Earth and Planetary Science Letters. 380, 98-111. https://doi.org/10.1016/j.epsl.2013.08.034

Lü, Y., Liu, B., Pei, S., Sun, Y., Toksoz, M.N., Zeng, X., 2012. Pn tomographic velocity and anisotropy beneath the Iran region. Bulletin of the Seismological Society of America. 102, 426-435. https://doi.org/10.1785/0120100141

Lü, Y., Ni, S., Chen, L., Chen, Q.-F., 2017. Pn tomography with Moho depth correction from eastern Europe to western China. Journal of Geophysical Research: Solid Earth. 122, 1284-1301. https://doi.org/10.1002/2016jb013052

Magni, V., Allen, M.B., van Hunen, J., Bouilhol, P., 2017. Continental underplating after slab break-off. Earth and Planetary Science Letters. 474, 59-67. https://doi.org/10.1016/j.epsl.2017.06.017

Mahmoodabadi, M., Yaminifard, F., Tatar, M., Kaviani, A., Motaghi, K., 2019. Upper-mantle velocity structure beneath the Zagros collision zone, Central Iran and Alborz from nonlinear teleseismic tomography. Geophysical Journal International. 218, 414-428. https://doi.org/10.1093/gji/ggz160

Manaman, N.S., Shomali, H., 2010. Upper mantle S-velocity structure and Moho depth variations across Zagros belt, Arabian–Eurasian plate boundary. Physics of the Earth and Planetary Interiors. 180, 92-103. https://doi.org/10.1016/j.pepi.2010.01.011

Manaman, N.S., Shomali, H., Koyi, H., 2011. New constraints on upper-mantle S-velocity structure and crustal thickness of the Iranian plateau using partitioned waveform inversion. Geophysical Journal International. 184, 247-267. https://doi.org/10.1111/j.1365-246X.2010.04822.x

Mooney, W.D., 2015. Crust and lithospheric structure—global crustal structure. Elsevier, Amsterdam.

Omrani, J., Agard, P., Whitechurch, H., Benoit, M., Prouteau, G., Jolivet, L., 2008. Arc-magmatism and subduction history beneath the Zagros Mountains, Iran: A new report of adakites and geodynamic consequences. Lithos. 106, 380-398. https://doi.org/10.1016/j.lithos.2008.09.008

Pei, S., Sun, Y., Toksöz, M.N., 2011. Tomographic Pn and Sn velocity beneath the continental collision zone from Alps to Himalaya. Journal of Geophysical Research. 116. https://doi.org/10.1029/2010jb007845

Rahmani, M., Motaghi, K., Ghods, A., Sobouti, F., Talebian, M., Ai, Y., Chen, L., 2019. Deep velocity image of the north Zagros collision zone (Iran) from regional and teleseismic tomography. Geophysical Journal International. 219, 1729-1740. https://doi.org/10.1093/gji/ggz393

Sadeghi-Bagherabadi, A., Sobouti, F., Ghods, A., Motaghi, K., Talebian, M., Chen, L., Jiang, M., Ai, Y., He, Y., 2018. Upper mantle anisotropy and deformation beneath the major thrust-and-fold belts of Zagros and Alborz and the Iranian Plateau. Geophysical Journal International. 214, 1913-1918. https://doi.org/10.1093/gji/ggy233

Shahabpour, J., 2007. Island-arc affinity of the Central Iranian Volcanic Belt. Journal of Asian Earth Sciences. 30, 652-665. https://doi.org/10.1016/j.jseaes.2007.02.004

Shomali, Z.H., Keshvari, F., Hassanzadeh, J., Mirzaei, N., 2011. Lithospheric structure beneath the Zagros collision zone resolved by non-linear teleseismic tomography. Geophysical Journal International. 187, 394-406. https://doi.org/10.1111/j.1365-246X.2011.05150.x

Stern, R.J., Moghadam, H.S., Pirouz, M., Mooney, W., 2021. The geodynamic evolution of Iran. Annual Review of Earth and Planetary Sciences. 49, 9-36. https://doi.org/10.1146/annurev-earth-071620-052109

Taghizadeh-Farahmand, F., Afsari, N., Sodoudi, F., 2015. Crustal thickness of Iran inferred from converted waves. Pure and Applied Geophysics. 172, 309-331. https://doi.org/10.1007/s00024-014-0901-0

van Hunen, J., Allen, M.B., 2011. Continental collision and slab break-off: A comparison of 3-D numerical models with observations. Earth and Planetary Science Letters. 302, 27-37. https://doi.org/10.1016/j.epsl.2010.11.035

Verdel, C., Wernicke, B.P., Hassanzadeh, J., Guest, B., 2011. A Paleogene extensional arc flare-up in Iran. Tectonics. 30, n/a-n/a. https://doi.org/10.1029/2010tc002809

Wang, X., Chen, L., Talebian, M., Ai, Y.S., Jiang, M.M., Yao, H.J., He, Y.M., Ghods, A., Sobouti, F., Wan, B., Chu, Y., Hou, G.B., Chen, Q.F., Chung, S.L., Xiao, W.J., Wu, F.Y., Zhu, R.X., 2022. Shallow Crustal Response to Arabia-Eurasia Convergence in Northwestern Iran: Constraints From Multifrequency P-Wave Receiver Functions. Journal of Geophysical Research-Solid Earth. 127. https://doi.org/10.1029/2022jb024515

Wortel, M.J.R., Spakman, W., 2000. Subduction and slab detachment in the Mediterranean-Carpathian region. Science. 290, 1910-1917. https://doi.org/10.1126/science.290.5498.1910

Wu, Z., Chen, L., Talebian, M., Wang, X., Jiang, M., Ai, Y., Lan, H., Gao, Y., Khatib, M.M., Hou, G., Chung, S.L., Liang, X., Zhao, L., Naimi-Ghassabian, N., Xiao, W., Zhu, R., 2021. Lateral structural variation of the lithosphere-asthenosphere system in the northeastern to eastern Iranian Plateau and Its tectonic implications. Journal of Geophysical Research: Solid Earth. 126. https://doi.org/10.1029/2020jb020256

Yang, G., Chen, L., Zhao, L.F., Xie, X.B., Yao, Z.X., 2023. Crustal Lg attenuation beneath the Iranian Plateau: Implications for Cenozoic magmatism related to slab subduction, slab break-off, and mantle flow. Journal of Geophysical Research: Solid Earth. 128. https://doi.org/10.1029/2022JB025664

Yang, G., Zhao, L.F., Xie, X.B., He, X., Lü, Y., Yao, Z.X., 2022. "Double Door" Opening of the Japan Sea Inferred by Pn Attenuation Tomography. Geophysical Research Letters. 49. https://doi.org/10.1029/2022gl099886

Yang, H., Zhang, H., Xiao, W., Tao, L., Gao, Z., Luo, B., Zhang, L., 2021. Multiple Early Paleozoic granitoids from the southeastern Qilian orogen, NW China: Magma responses to slab roll-back and break-off. Lithos. 380-381. https://doi.org/10.1016/j.lithos.2020.105910

Zhao, L.F., Xie, X.B., Tian, B.F., Chen, Q.F., Hao, T.Y., Yao, Z.X., 2015. Pn wave geometrical spreading and attenuation in Northeast China and the Korean Peninsula constrained by observations from North Korean nuclear explosions. Journal of Geophysical Research: Solid Earth. 120, 7558-7571. https://doi.org/10.1002/2015jb012205

Zhu, H., Bozdağ, E., Duffy, T.S., Tromp, J., 2013. Seismic attenuation beneath Europe and the North Atlantic: Implications for water in the mantle. Earth and Planetary Science Letters. 381, 1-11. https://doi.org/10.1016/j.epsl.2013.08.030